JOURNAL OF MATERIALS SCIENCE 23 (1988) 2897–2904

Processing of anatase prepared from hydrothermally treated alkoxy-derived hydrous titania

Y. OGURI*, R. E. RIMAN‡, H. K. BOWEN
Ceramics Processing Research Laboratory, Materials Processing Center, Massachusetts Institute of Technology, Cambridge, Massachusetts 02139, USA

Spherical, submicrometre, amorphous hydrous titania powder synthesized by controlled hydrolysis and polymerization from titanium tetraethoxide solutions was hydrothermally converted to spherical polycrystalline anatase particles by autoclaving or refluxing. Green compacts produced with either autoclaved or refluxed powder via a colloid filtration route had a high density and were crack-free; processing with untreated hydrous titania resulted in cracked green compacts. Compacts of the hydrothermally treated powders could be sintered to 98% theoretical density at temperatures as low as 900° C. A compact of commercial powder produced in the same fashion was not observed to densify at such temperatures. Using various firing techniques, compacts of the hydrothermally treated powder could be sintered to 98% theoretical density or greater while controlling the titania phase assemblage as (1) anatase, (2) rutile, or (3) a mixture of anatase and rutile. By scaling the phase transformation and sintering kinetics, the grain size of the sintered microstructure can be controlled from a submicrometre to a micrometre scale.

1. Introduction

Control of the physical and chemical characteristics of ceramic powders is receiving attention because of the role these characteristics play in determining green microstructure uniformity and density [1]. Significant advances have been made on the low-temperature solid-state sintering of TiO_2 [2–4], a ceramic material used in the form of anatase or rutile in paint, electronic, and catalytic applications [5]. However, green compacts consisting of submicrometre, spherical, unagglomerated, narrow-size-distribution, alkoxy-derived hydrous titania used in the cited studies can crack during the drying or firing stages because of dimensional changes in the particles caused by the evolution of volatile species produced by occluded solvent, water, and decomposing hydroxide and alkoxide species. Conversion of hydrous titania to a dense ceramic oxide, TiO_2, circumvents cracking caused by these chemical and physical factors.

Conversion of hydrous titania to TiO_2 can be accomplished in two ways. Calcination processes can convert hydrous titania to TiO_2 at temperatures as low as 350° C [6]. However, calcination processes cause particles to form aggregates of primary particles which cannot be redispersed (hard agglomerates) [7]. On the other hand, hydrothermal treatment in aqueous media [8] can convert the ideal powder to a crystalline oxide without a dramatic change in its physical characteristics. Furthermore, this dispersion of crystalline oxide is a convenient medium to use for subsequent processing steps, such as colloid filtration to produce green compacts.

This study describes the preparation and packing of hydrothermally treated, alkoxy-derived anatase. The sinterability of this powder allows densification to take place while maintaining the titania phase as either (1) anatase, (2) rutile, or (3) a mixture of anatase and rutile. Previous works have focused on the phase transformation of anatase to rutile in powders [5, 9, 10] or single crystals [11]. This study demonstrates how this transformation can be used as a means for controlling the grain size of the sintered microstructure.

2. Experimental procedure

The procedure followed in this study is summarized by the flow chart in Fig. 1. The reactants consisted of two streams: a "wet" stream, consisting of ethanol and water, and a "dry" stream, consisting of titanium ethoxide (Kay-Fries, Rockleigh, New Jersey), and ethanol (dehydrated 200-proof, Pharmco Publicker Ind. Inc, Dayton, New Jersey). These two streams were filtered (0.3 μm Balston filter) then pumped in a predetermined molar ratio to a static mixer, from which the combined stream entered a continuous-flow reactor designed by Novich [12] and modified by Nahass and Bowen [13]. For this study, a molar ratio of water to titanium tetraethoxide of 4.3 was selected, with an alkoxide concentration of 0.23 M.

* *Present address*: Mitsubshi Chemical Industries Limited, 1000 Kamoshida-cho, Midori-Ku, Yokohama City, Kanagawa 227, Japan.
‡ *Present address*: Rutgers, the State University of New Jersey, College of Engineering, Brett and Bowser Roads, Piscataway, New Jersey, USA.

0022–2461/88 $03.00 + .12

TABLE I Synthesis conditions and physical characteristics of alkoxy-derived hydrous titania

Synthesis conditions	Powder properties					
	Phase	Specific surface area ($m^2 g^{-1}$)	Mean diameter (μm)	Shape	Size distribution (μm)	Density [2] ($g ml^{-1}$)
$[H_2O]:[Ti(OC_2H_5)_4]$ (molar ratio) 0.98:0.23	amorphous	323	0.69	spheroidal	0.3–0.8	3.1

The continuous-flow reactor design was adjusted to allow an average reactant residence time in the static mixer of 11.9 sec.

The precipitate produced in the reactor was washed (i.e. centrifuged and redispersed) with ethanol once, and with deionized water three times; the solution pH was then adjusted to 10 by adding ammonium hydroxide. Table I summarizes the physical properties of the amorphous powder synthesized.

The resulting slurry's solid content was adjusted to 5 wt %, and the slurry was then divided into three batches. One batch was poured into an autoclave (Fig. 2), the second was refluxed in a condenser (Fig. 3), and the third was given no thermal treatment.

Table II summarizes the hydrothermal conditions used for each autoclaving experiment. In each case, the autoclaving temperature was measured by a chromel–alumel thermocouple, and pressure was determined by a Bourdon-tube pressure gauge. After cooling, the slurry was removed from the autoclave and characterized by X-ray diffraction, electron diffraction, scanning electron microscopy, bright-field transmission electron microscopy, photon correlation spectroscopy, BET surface area analysis, infrared spectroscopy, carbon–hydrogen analysis, and thermal analysis.

Powder compacts were prepared from the slurry using the following method. A 5 wt % slurry was poured through an open-bottomed glass tube (i.d. = 14.5 mm) into an attached plastic funnel fitted with a 0.3 μm filter. The column was then evacuated through the funnel until water was no longer observed on the filter cake's surface. The resulting compacts (each 3 to 4 mm thick) were dried in air at 25 $\pm$ 1° C, then sintered.

Table III summarizes the hydrothermal conditions used for each refluxing experiment. After refluxing, each slurry was characterized and compacted by the same methods as were used for the autoclaved slurries.

TABLE II Experimental conditions for autoclaved alkoxy-derived hydrous titania

	Run no.		
	1	2	3
Temperature (° C)	200	253	282
Pressure (MPa)	1.6	4.2	6.6
Time (h)	5	5	5
Phase	anatase	anatase	anatase
Crystallite size* (nm)	12	14	18
Surface area ($m^2 g^{-1}$)	110	90	71
Particle size† (nm)	14	17	22
Particle shape	RB‡	RB	RB

*Determined by X-ray diffraction.
†Determined by BET method.
‡Raspberry-like in appearance.

3. Results and discussion

3.1. Physical characterization of powders

The physical characteristics of the hydrothermally treated powders were determined using electron microscopy, X-ray diffraction, and specific surface area measurements.

3.1.1. Autoclaved powder

Results of autoclaving the alkoxide-derived TiO_2 powders are summarized in Table II. X-ray and electron diffraction analysis showed that the amorphous TiO_2 in all cases crystallized. *d*-spacings calculated from X-ray diffraction patterns corresponded to those of the anatase phase.

The hydrothermal conversion of the amorphous powder to the anatase phase was monitored with electron microscopy. The scanning electron micrograph (SEM) in Fig. 4 shows amorphous TiO_2 particles before hydrothermal treatment. The SEMs in Fig. 5 and the transmission electron micrograph (TEM) in Fig. 6a demonstrate that after the powder was autoclaved at 253° C and 4.2 MPa for 5 h, each particle appeared as a polycrystalline sphere comprising small grains of ~ 10 nm diameter. The electron diffraction pattern of the autoclaved powder (Fig. 6b) shows these granules to be crystalline and corresponding to the anatase phase.

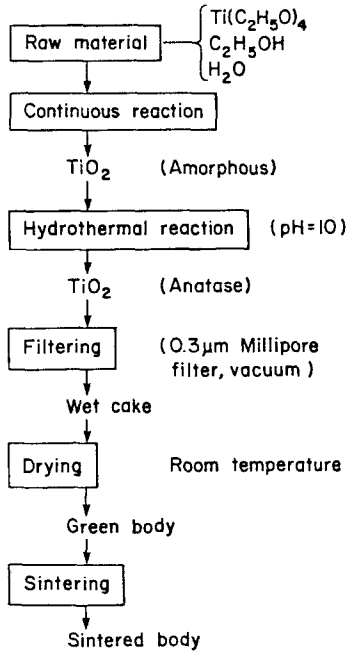

Figure 1 Flow diagram of the general procedure used for the processing of hydrothermally treated powders.

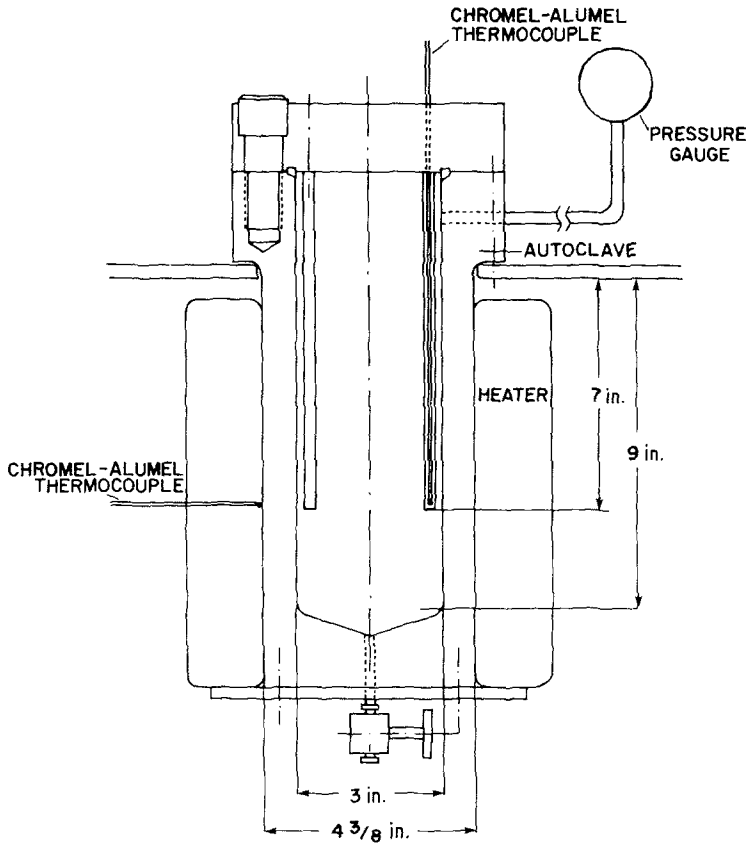

Figure 2 Schematic drawing of 1 litre autoclave used for hydrothermal treatment.

Specific surface areas were found to decrease with increasing autoclave temperature and pressure. Using the density of single-crystal anatase, the calculated average particle size was found to agree fairly well with the crystallite size as determined by X-ray diffraction line broadening (Table II). The increase in particle size and decrease in surface area were attributed to coarsening of the granules (crystallites) in each particle.

3.1.2. Refluxed powder

Table III shows the results of refluxing the synthesized amorphous powder. After 1 h refluxing, the powder remained entirely unchanged; after 12 h, an anatase peak was detected by X-ray diffraction analysis; and after 36 h refluxing, the powder had transformed completely to anatase.

Refluxing is essential for anatase crystallization. Powders refluxed in deionized water crystallized, but untreated samples aged for 3 months in pH 10 water did not crystallize and exhibited the same thermal analysis trace as described previously for the untreated powder.

Fig. 7a is a TEM taken of powder refluxed for 48 h. The electron diffraction pattern of this powder (Fig. 7b) has well-defined diffraction rings as opposed to the more spotted pattern observed for the autoclaved powder (Fig. 6b). These data indicate that the crystallite size of the refluxed powder is smaller than that of the autoclaved powder. This interpretation is supported by surface area measurements of the refluxed powder which were consistently higher than those of the autoclaved powder (Table III).

TABLE III Experimental conditions and characteristics of refluxed alkoxy-derived hydrous titania

	Run no.			
	1	2	3	4
Temperature (°C)	100	100	100	100
Pressure (MPa)	0.1	0.1	0.1	0.1
Time (h)	1	12	36	48
Phase	AMO*	AT†	AT	AT
Surface area ($m^2 g^{-1}$)	–	215	–	182
Particle size (nm)‡	–	7.2	–	8.5

*Amorphous.
†Anatase.
‡Calculated from surface area measurements.

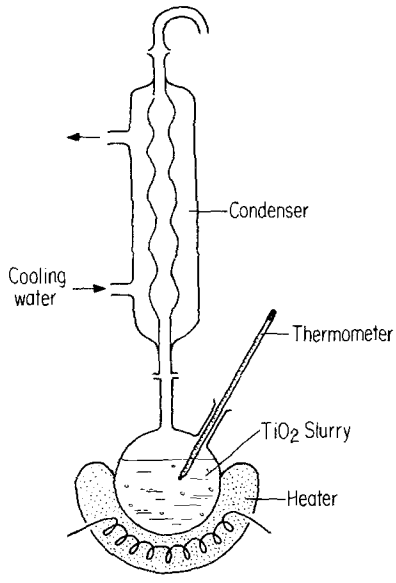

Figure 3 Refluxing apparatus used for hydrothermal treatment.

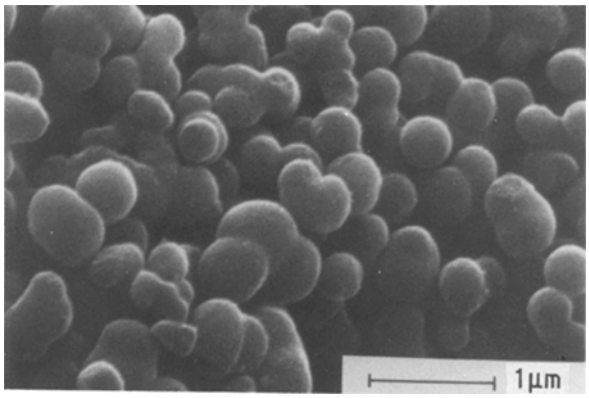

Figure 4 Scanning electron micrograph of hydrous titania prepared from hydrolysis and polymerization of titanium tetraethoxide.

Table III also shows how the powder surface area decreased as the refluxing time was increased from 12 to 48 h. As observed in the autoclaved powder, an increase in the granule (crystallite) size due to coarsening would account for the decrease in surface area.

3.2. Chemical characterization of powders

Infrared analysis, carbon–hydrogen analyses, differential thermal analysis, and thermal gravimetric analysis were performed on both untreated and treated powders that had been aged in air for more than 6 months.

Infrared analysis of Fluorolube mulls prepared in air revealed that all three powders had the same compositional features. Infrared transmission scans done in the range 4000 to 1300 cm^{-1} revealed that water and hydroxyl groups were present, as indicated by absorption bands at 1640 and approximately 3300 cm^{-1}, respectively. The absence of C–H stretches at approximately 2900 cm^{-1} showed that few if any organics were present [14, 15]. These results were supported by carbon–hydrogen analysis, which showed that low or immeasurable levels of carbon were present (untreated powder, 0.40 wt % C; autoclaved powder, 0.62 wt % C; refluxed powder, 0.00 wt % C). The untreated powder contained four times more hydrogen (2.22 wt %) than did the treated powders, which shows that the untreated powder contained a significantly higher concentration of Ti–OH and water, as expected for hydrous titania.

Differential thermal analysis of the three powders revealed several differences between them. In the differential thermal analysis trace, the untreated powder exhibited a large exothermic peak near 400° C while samples that were refluxed or autoclaved showed no peak. This exothermic peak is probably due to the condensation of Ti–OH groups with the consequent release of water and formation of anatase, because hydrous titania prepared via various synthetic methods forms TiO_2 at this approximate temperature [6]. All three samples exhibited a small endothermic peak below 100° C which can be attributed to the release of adsorbed water.

Thermal gravimetric analysis of the three powders revealed other compositional differences. When powders were heated to 900° C, the untreated powder exhibited a total weight loss of 9 wt % while autoclaved and refluxed powders each had a total weight loss of only 4 wt %. All weight was lost below 450° C in each case. Hydrogen analysis indicated that the untreated powder should have exhibited a total weight loss of 20 wt % while the refluxed and autoclaved powders should each have shown a weight loss of 5 wt %. The lack of agreement between the thermal gravimetric and hydrogen analysis results obtained for the untreated powder, compared to the reasonable agreement between the results obtained for the treated powders, shows that the untreated powder is considerably more hygroscopic than the treated powder.

In summary, the thermal analysis results in conjunction with other data showed that the untreated powder underwent a chemical reaction that did not occur with the refluxed or autoclaved powders. This reaction is believed to have already taken place in the autoclaved or refluxed powders, and is responsible for the crystallization of the powder.

3.3. Powder crystallization model

The X-ray diffraction, weight loss, infrared spectrum, and carbon–hydrogen analysis data obtained for the untreated powder are characteristic of hydrous titania, which consists of a highly cross-linked Ti–O network containing both Ti–OH and water. The X-ray diffraction, weight loss, infrared, and carbon–hydrogen analysis data obtained for the treated powders suggest that the number of Ti–OH groups was reduced, with surface-adsorbed water remaining.

From the above data, a model for the crystallization

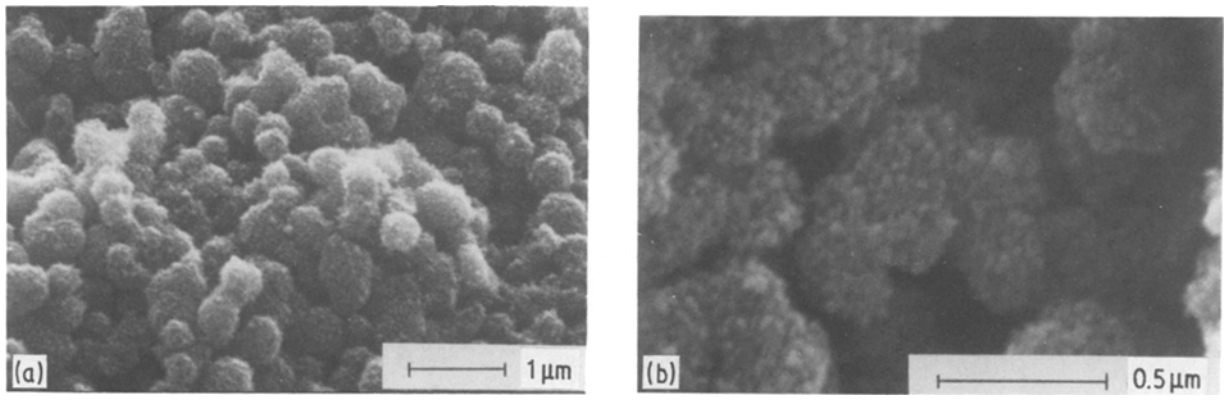

Figure 5 Scanning electron micrographs of alkoxide-derived titania powder after autoclaving (run 2): (a) × 17 300, (b) × 58 500.

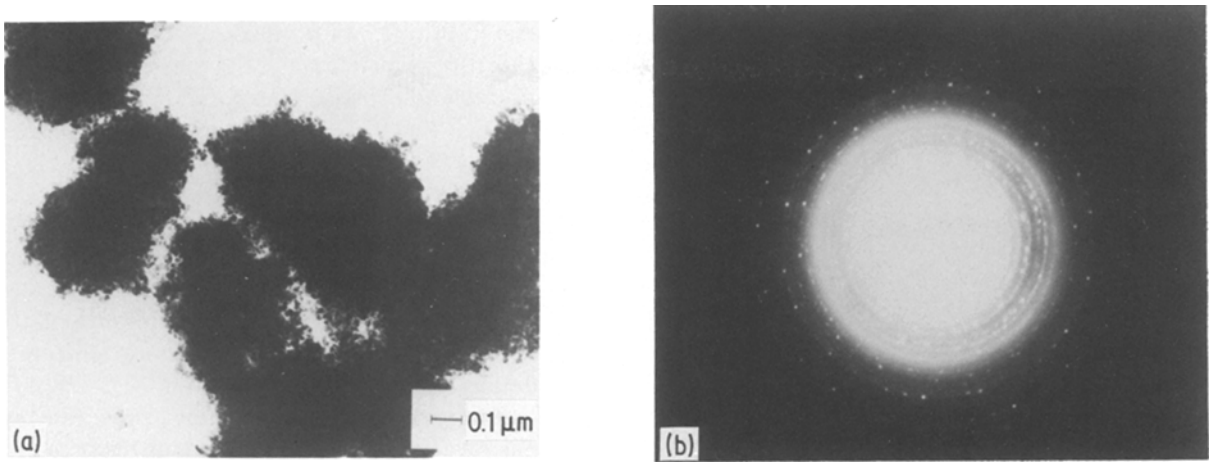

Figure 6 (a) Transmission electron micrograph and (b) electron diffraction pattern of alkoxide-derived titania powder after autoclaving (run 2).

of alkoxy-derived hydrous titania can be developed. During hydrolysis and polymerization, the reaction in nonaqueous media precipitates hydrous titania containing ethoxide groups, hydroxyl groups, bridging oxygens, and probably a small amount of water

$$Ti(OEt)_4 + uH_2O \rightarrow TiO_x(OH)_y(OEt)_z + vEtOH \quad (1)$$

During the rinsing and dispersion steps, the surface ethoxide groups are converted to hydroxyl groups, and water can adsorb onto the powder surface:

$$TiO_x(OH)_y(OEt)_z + nH_2O \rightarrow TiO_x(OH)_{(y+z)} + nEtOH \quad (2)$$

$$TiO_x(OH)_{(y+z)} + rH_2O \rightarrow TiO_x(OH)_{(y+z)} \cdot rH_2O \quad (3)$$

Because the powder contains no organic species, crystallization can be attributed to thermally activated condensation reactions which cross-link the $TiO_x(OH)_{(x+z)}$ polymer and release water. When the cross-linking is extensive enough, the anatase phase can nucleate and grow

$$O_x(OH)_{(x+z-1)}Ti\text{–}OH + HO\text{–}TiO_x(OH)_{(x+z-1)} \rightarrow O_x(OH)_{(x+z-1)}Ti\text{–}O\text{–}TiO_x(OH)_{(x+z-1)} + H_2O \quad (4)$$

The formation of polycrystalline particles is attributed to multiple regions of the particle where hydrolysis polymers are more condensed than other regions. These regions crystallize before the less condensed regions, leading to multiple nucleation sites for the anatase phase.

3.4. Wet cake properties

Filter-casting studies of the three powders exhibited significant differences in their processability. Compacts prepared with the untreated hydrous oxide powder formed hard and brittle bodies which cracked upon drying, with densities 30 to 40% theoretical (hydrous titania = 3.1 g ml^{-1}) [2]. On the other hand, powders which were autoclaved or refluxed and filter-cast into plastic cakes, dried without cracking to densities of 50 to 55% theoretical. In general, it was observed that ultrasonic treatment of the hydrothermally treated dispersions broke the polycrystalline particles into their discreet unit crystallites while the untreated hydrous oxide powders retained their integrity. Fig. 8 shows how the fine crystallites of the treated powder could be cast to form a uniform green microstructure.

Two factors may account for the above observed differences. First, surface area may be important. The untreated powder has a microporous surface (Table I)

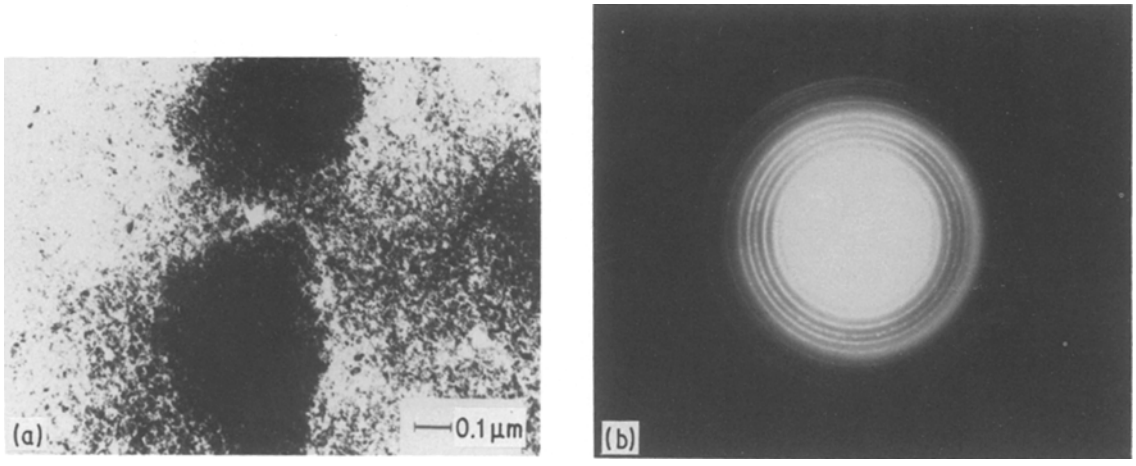

Figure 7 (a) Transmission electron micrograph and (b) electron diffraction pattern of alkoxide-derived powder after refluxing (run 4).

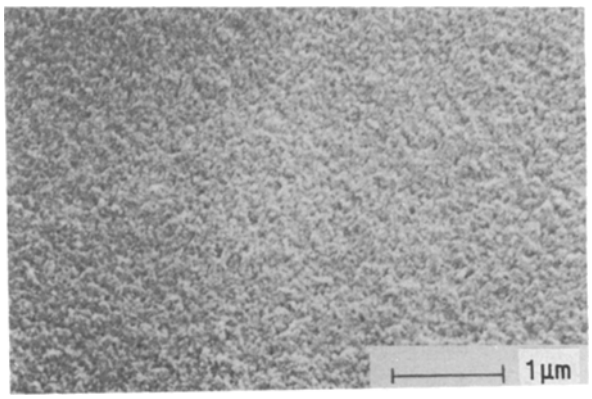

Figure 8 Scanning electron micrograph of anatase green compact fracture surface made from alkoxide-derived powder after autoclaving (run 2).

with a higher surface area than the treated powders, which consist of polycrystalline particles. The higher surface areas lead to larger capillary forces or differential strains, which exert tensile stresses that can crack the compact. However, cracking is more likely due to the substantial reduction in size the untreated particles undergo while drying. The condensed $TiO_x(OH)_y$ polymers in each particle may be solvated by the dispersion medium and substantially recoil during drying, leading to a larger volume change of each particle and hence a large degree of drying shrinkage. Another factor leading to shrinkage of the hydrous oxide particles could be the evolution of water due to condensation between Ti–OH groups or the release of molecularly associated water. Particle shrinkage is not significant in the case of the treated powders because the dense crystallites only lose surface-adsorbed water during drying, resulting in a smaller degree of drying shrinkage.

3.5 Sintering behaviour

All bodies were sintered in air and their microstructures characterized using scanning electron microscopy, quantitative X-ray diffraction, dilatometry, and density measurements using Archimedes' method. Refluxed and autoclaved powders exhibited similar sintering behaviour. The following experiments were performed using autoclaved powder (run 2). Control of the heating schedule allowed bodies to densify as (1) anatase, (2) rutile, or (3) a mixture of these two phases because the relative rates of sintering (R_S) and the anatase-to-rutile phase transformation (R_T) can be scaled such that $R_S \gg R_T$, $R_S \simeq R_T$, or $R_S \ll R_T$.

3.5.1. Anatase sintering ($R_S \gg R_T$)

For these studies, filtercast green bodies utilizing autoclaved powder or commercially obtained anatase powder (New Jersey Zinc Co., Inc., Palmerton, Pennsylvania) were sintered using a heating rate of 10° C min^{-1} to 900° C, and cooled to room temperature inside the dilatometer.

Sintering studies under the above processing conditions revealed several advantageous features of the autoclaved powders. First, dense anatase bodies were obtained. Fig. 9a shows the fracture surface of a body identified with X-ray diffraction as anatase that sintered to 98% theoretical. Second, both the fracture surface and a polished section thermally etched at 880° C for 20 min (Fig. 10) reveals that the microstructure consists of submicrometre grains with no evidence of secondary grain growth. Finally, compacts of the autoclaved powder sintered better than did commercially obtained TiO_2 processed in the same manner (Fig. 9b). Compacts of the commercial powder with a green density of 45% theoretical failed to sinter despite the submicrometre particle size and reasonably high green density. Dilatometry studies revealed that the autoclaved powder sinters at a temperature ~ 400° C lower than does the commercially obtained powder (Fig. 11).

The enhanced sinterability of this powder and the uniform microstructure obtained from the autoclaved powder can be attributed to the small size of anatase crystallites and their uniform packing in the green compact. It is also important to note that the hydrothermally treated powder sintered extensively in the range of the equilibrium anatase-to-rutile phase transformation temperature [10] while the kinetics of this transformation proceeded relatively slowly ($R_S \gg R_T$). Sluggish transformation kinetics have been observed for chemically derived [5] and commercially available powders [10] in the submicrometre range. The literature also shows that the transformation rate

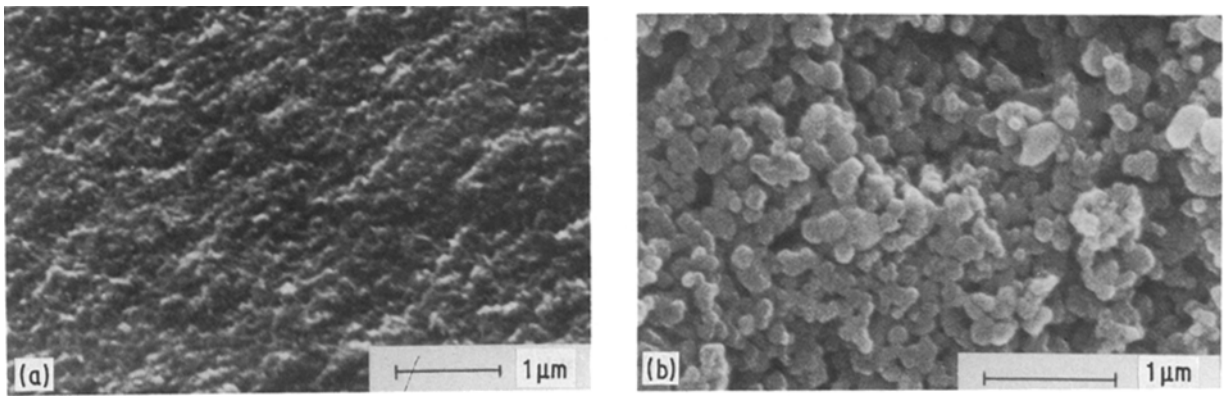

Figure 9 Scanning electron micrographs of the fracture surface of a sintered compact: (a) anatase body produced from autoclaved powder and (b) anatase body produced from commercial powder.

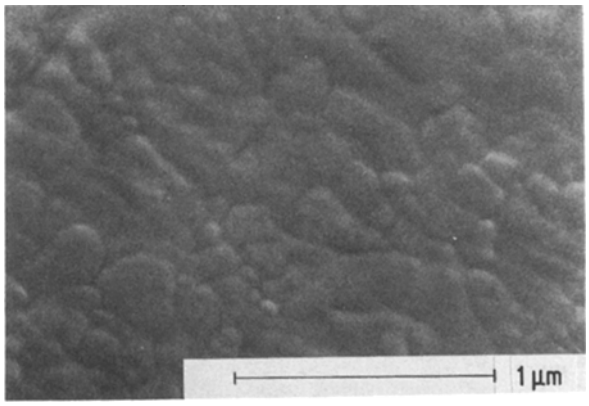

Figure 10 Scanning electron micrograph of a thermally etched, polished section of the sintered anatase body shown in Fig. 9.

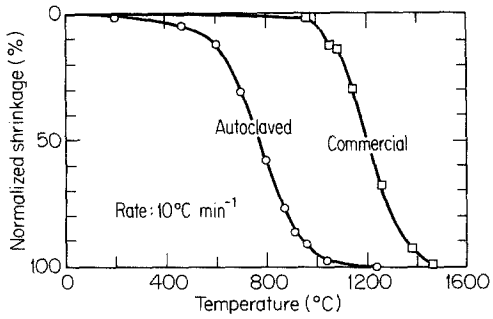

Figure 11 Normalized shrinkage of autoclaved and commercial anatase TiO_2 compacts as a function of temperature for a constant heating rate of 10° C min^{-1}.

increases dramatically as the temperature exceeds ~900° C. Similar observations were made in this work as described below.

3.5.2. Sintering with an anatase-to-rutile phase transformation ($R_S \simeq R_T$)

In this study, anatase bodies sintered as described in Section 3.5.1 were heated a second time. Samples were heated at a rate of 10° C min^{-1} to 900° C and annealed at the temperatures and for the time periods specified in Table IV.

The photomicrographs and X-ray diffraction and density measurements reveal two important features imparted by annealing. Table IV shows that the annealing treatment controls not only the degree of densification, but more importantly, the molar ratio of rutile to anatase. This is because the relative rates of sintering and the anatase-to-rutile phase transformation are comparable ($R_S \simeq R_T$). Previous characterization showed that the anatase grains were on the submicrometre scale. Fracture surfaces of the various samples show that the fraction of anatase determined by X-ray diffraction is proportional to the fine-grain structure, as shown in Fig. 12. Thus, it seems logical to assume that the micrometre-scale smooth surfaces are indicative of large rutile grains that have nucleated and grown. These results signify that annealing treatments of presintered anatase bodies are useful for producing microstructures with bimodal grain-size distributions with the two distributions in a controlled ratio.

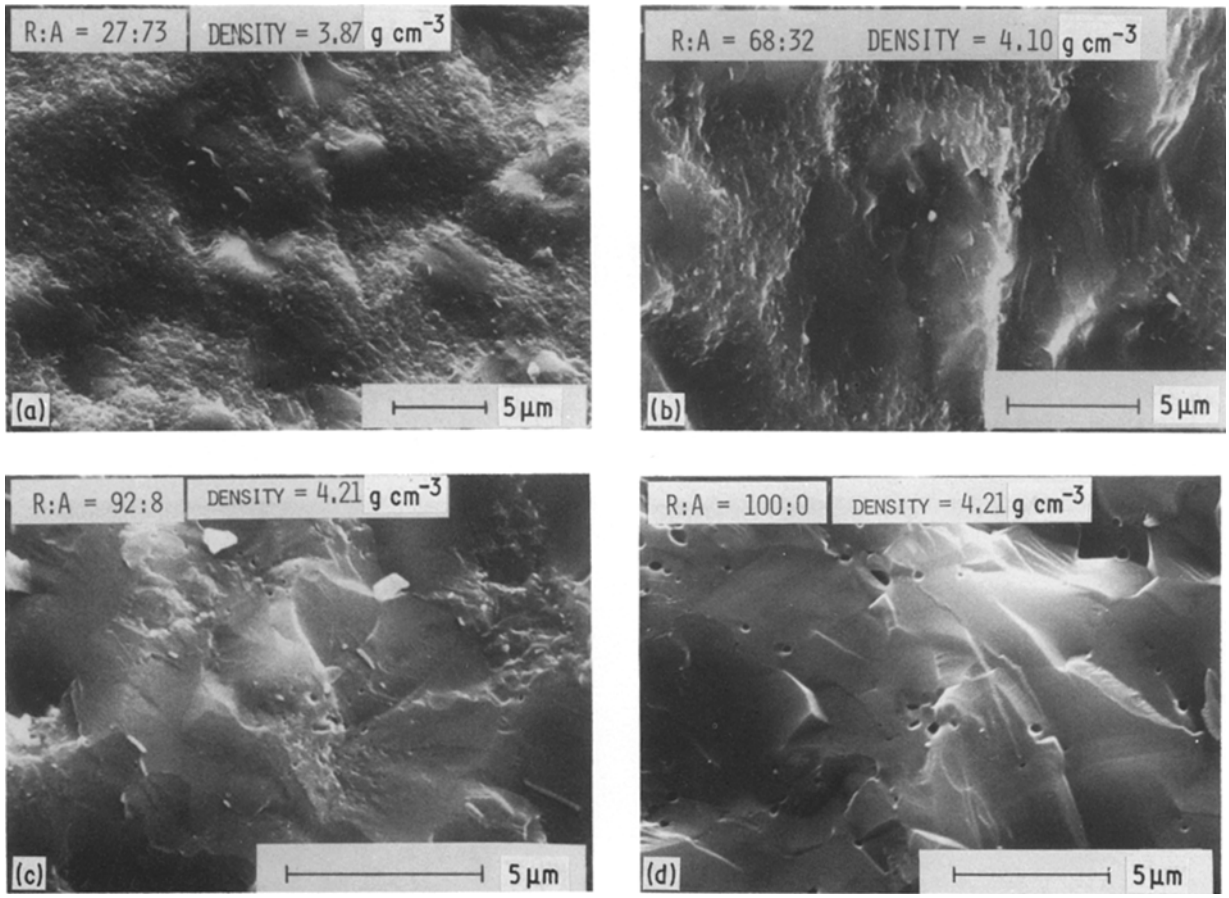

Figure 12 Scanning electron micrographs of TiO_2 sintered body processed as described in Section 3.5.2, using annealing temperatures and times of (a) 850° C, 5 h, (b) 1000° C, 0.5 h, (c) 1000° C, 1 h, and (d) 1240° C, 0 h (R : A denotes the rutile : anatase phase ratio).

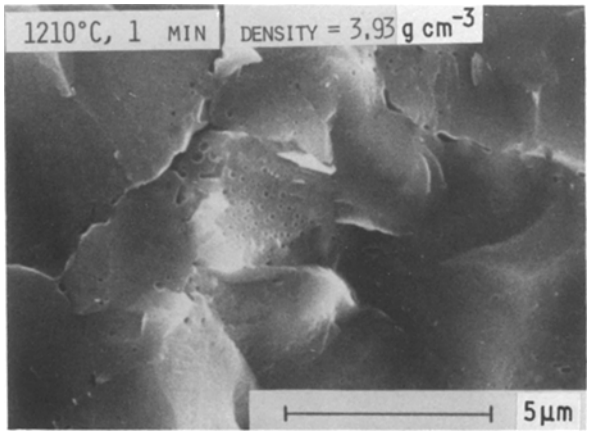

Figure 13 Scanning electron micrograph showing the microstructure of a TiO_2 body fast-fired at 1210° C for 1 min.

3.5.3. Rutile sintering ($R_T \gg R_S$)

In this study, anatase bodies sintered as described in Section 3.5.1 were heated a second time by soaking at 1210° C for a duration of 1, 3, or 5 min (fast firing).

The fast-fired samples behaved in a different manner than did the samples described in Section 3.5.2. Table V indicates that samples consisted of single-phase rutile and were considerably densified. Fig. 13 shows how the grain size in all samples was on a micrometre scale, which is expected for microstructures which nucleate and grow the rutile phase. The phase assemblage and the increase in density shown in Table V indicate that the kinetics of the phase transformation was more rapid than the densification rate. In addition, secondary fast-firing treatments are a good means for obtaining rutile bodies with micrometre grain sizes.

4. Conclusions

It is concluded that the role and benefits of hydrothermal processing of alkoxide-derived hydrous titania powder are now better understood. Autoclaving or refluxing imparts important physical and chemical changes to the powder. The hydrous oxide chemically converts to anatase due to thermally activated condensation reactions which crosslink the $TiO_x(OH)_y$ polymers. Homogeneous, spherical, amorphous, alkoxy-derived hydrous titania physically converts to spherical polycrystalline anatase particles. The hydrothermally processed powder is of great utility because (1) crack-free green bodies can be filtercast, unlike untreated powder, (2) the powder is extremely sinterable, and (3) the relative rates of phase transformation and densification can be controlled to modify phase distribution and grain size.

TABLE IV Densification and transformation characteristics of anatase bodies after a second heating and annealing at selected temperatures, for selected time periods

Sample	Temp. (° C)	Time (h)	Rutile : anatase*	% $\varrho_{th}^{\dagger}$
1	850	5	27 : 73	97.2
2	1000	0.5	68 : 32	99.5
3	1000	1.0	92 : 8	100
4	1240	0	100 : 0	99.3

*Molar or mass ratio of rutile to anatase.
† % ϱ_{th} calculation based on theoretical density of the phase mixture indicated by the rutile : anatase ratio.

TABLE V Density and phase of samples fast-fired at 1210° C for selected time periods

Sample	Time (min)	Phase	ϱ_{exp}	% ϱ_{th}
1	1	Rutile	3.93	92.7
2	3	Rutile	3.98	93.9
3	5	Rutile	4.24	100

Acknowledgements

This research was sponsored by the Air Force Office of Scientific Research, Chemical Sciences Division, under contract No. AFOSR-83-0192, and by the MIT-Industry Ceramics Processing Research Consortium. The authors wish to thank E. A. Barringer for providing valuable information, B. Novich and P. Nahass for preparing the powders, and J. Stitt for reviewing the manuscript.

References

1. H. K. BOWEN, *J. Mater. Sci. Engng* **44** (1980) 1.
2. E. A. BARRINGER and H. K. BOWEN, *Langmuir* **1** (1985) 414.
3. *Idem, J. Amer. Ceram. Soc.* **65** (1982) C199.
4. E. A. BARRINGER, R. BROOK and H. K. BOWEN, in "Sintering and Heterogeneous Catalysis", edited by G. C. Kuczynski, A. E. Miller, and G. A. Sargent (Plenum, New York, 1984) pp. 1–21.
5. Y. IIDA and S. OZAKI, *J. Amer. Ceram. Soc.* **44** (1961) 120.
6. L. ERDEY, "Gravimetric Analysis" (Pergamon, New York, 1965) pp. 459–73.
7. M. F. YAN and W. W. RHODES, *Mater. Sci. Engng* **61** (1983) 59.
8. A. MATTHEWS, *Amer. Mineral.* **61** (1976) 419.
9. A. W. CZANDERNA, C. N. R. RAO and J. M. HONING, *Trans. Faraday Soc.* **54** (1958) 1069.
10. S. HISITA, I. MUTOH, K. KOUMOTO and H. YANAGIDA, *Ceram. In.* **9** (2) (1983) 61.
11. R. D. SHANNON and J. A. PASK, *Amer. Mineral.* **49** (1964) 1707.
12. B. NOVICH, "Continuous Processing of Ceramic Oxide Powders," Report no. Q1, Ceramics Processing Research Laboratory, MIT, Cambridge, Massachusetts 02139 (1984).
13. P. NAHASS and H. K. BOWEN, *Mater. Sci. Engng* (1988) to be published.
14. L. J. BELLAMY, "The Infra-red Spectra of Complex Molecules" (Wiley, New York, 1975).
15. K. NAKAMOTO, "Infrared and Raman Spectra of Inorganic and Coordination Compounds" (Wiley, New York, 1978).

Received 2 September
and accepted 1 December 1987